ADVANCED MATERIALS

www.advmat.de

An Efficient, "Burn in" Free Organic Solar Cell Employing a Nonfullerene Electron Acceptor

*Hyojung Cha, Jiaying Wu, Andrew Wadsworth, Jade Nagitta, Saurav Limbu, Sebastian Pont, Zhe Li, Justin Searle, Mark F. Wyatt, Derya Baran, Ji-Seon Kim, Iain McCulloch, and James R. Durrant**

A comparison of the efficiency, stability, and photophysics of organic solar cells employing poly[(5,6-difluoro-2,1,3-benzothiadiazol-4,7-diyl)-alt-(3,3‴-di(2-octyldodecyl)-2,2′;5′,2″;5″,2‴-quaterthiophen-5,5‴-diyl)] (PffBT4T-2OD) as a donor polymer blended with either the nonfullerene acceptor EH-IDTBR or the fullerene derivative, [6,6]-phenyl C_{71} butyric acid methyl ester ($PC_{71}BM$) as electron acceptors is reported. Inverted PffBT4T-2OD:EH-IDTBR blend solar cell fabricated without any processing additive achieves power conversion efficiencies (PCEs) of 9.5 ± 0.2%. The devices exhibit a high open circuit voltage of 1.08 ± 0.01 V, attributed to the high lowest unoccupied molecular orbital (LUMO) level of EH-IDTBR. Photoluminescence quenching and transient absorption data are employed to elucidate the ultrafast kinetics and efficiencies of charge separation in both blends, with PffBT4T-2OD exciton diffusion kinetics within polymer domains, and geminate recombination losses following exciton separation being identified as key factors determining the efficiency of photocurrent generation. Remarkably, while encapsulated PffBT4T-2OD:$PC_{71}BM$ solar cells show significant efficiency loss under simulated solar irradiation ("burn in" degradation) due to the trap-assisted recombination through increased photoinduced trap states, PffBT4T-2OD:EH-IDTBR solar cell shows negligible burn in efficiency loss. Furthermore, PffBT4T-2OD:EH-IDTBR solar cells are found to be substantially more stable under 85 °C thermal stress than PffBT4T-2OD:$PC_{71}BM$ devices.

Organic solar cells (OSCs) require both efficient and stable operation to become viable for commercial application.[1] However, many organic photoactive materials and blends are susceptible to a range of light induced degradation mechanisms which often results in a significant decrease in the solar cell performance under solar irradiation.[2] In particular, bulk heterojunction OSCs incorporating C_{60}-based fullerene electron acceptors often show a significant initial loss of performance under sunlight exposure on a timescale of tens of hours before stabilizing at an efficiency 25%–50% lower than the initial value—a loss of performance widely referred to as "burn in."[3] Several possible origins of burn-in efficiency loss have been discussed in the literature,[2] including metal ion migration from device contacts,[4] photoinduced fullerene dimerization,[5] the photogeneration of electronic trap states,[6] and most recently spinodal demixing.[7] Thermally induced performance degradation has also been identified as significant issue for many OSCs and attributed primarily to thermally induced fullerene aggregation/crystallization; under modest thermal stress conditions, limited photoinduced fullerene dimerization has been reported to beneficial for device stability.[8] A further stability consideration is the use of process additives such diiodooctane (DIO),

Dr. H. Cha, J. Wu, A. Wadsworth, J. Nagitta, S. Pont, Prof. I. McCulloch, Prof. J. R. Durrant
Department of Chemistry and Centre for Plastic Electronics
Imperial College London
London SW7 2AZ, UK
E-mail: j.durrant@imperial.ac.uk

S. Limbu, Prof. J.-S. Kim
Department of Physics and Centre for Plastic Electronics
Imperial College London
London SW7 2AZ, UK

Dr. Z. Li, Dr. J. Searle, Prof. J. R. Durrant
SPECIFIC IKC
College of Engineering, Swansea University
Baglan Bay Innovation Centre
Port Talbot, Swansea SA12 7AX, UK

Dr. M. F. Wyatt
EPSRC UK National Mass Spectrometry Facility (NMSF)
Swansea University Medical School
Singleton Park, Swansea SA2 8PP, UK

Prof. D. Baran, Prof. I. McCulloch
Physical Sciences and Engineering Division
KAUST Solar Center (KSC)
King Abdullah University of Science and Technology (KAUST)
Thuwal 23955-6900, Kingdom of Saudi Arabia

DOI: 10.1002/adma.201701156

such additives are widely used to increase the efficiency of polymer:fullerene solar cells, but have also been shown to impact detrimentally on device stability.[9] As such the development of efficient organic solar cells which exhibit stable performance without significant burn-in loss remains a significant challenge in this field.

The last two years have seen rapid progress in the development of nonfullerene acceptors (NFAs) for bulk heterojunction organic solar cells, yielding device efficiencies over 11%.[10] Such NFAs can exhibit several potentially attractive features for organic solar cell application: strong and tunable light absorption, tunable molecular energy levels, and lower cost synthesis.[11] Given the greater synthetic flexibility of NFAs compared to fullerene acceptors, it is interesting to consider whether such OSCs employing NFAs can exhibit reduced burn-in degradation losses compared to fullerene acceptors, a subject to our knowledge not yet addressed in the literature to date.

We have recently reported a range of rhodanine-based NFAs which have achieved very promising device efficiencies in blends with P3HT, with efficiencies for ternary blends of up to 7.7%.[12–15] Such blends with P3HT have also shown promising unencapsulated device stabilities, significantly improved compared to those of analogous $PC_{61}BM$ devices, and indicative of promising resistance to oxygen and water induced degradation.[13] We have moreover shown that the replacement of P3HT with a lower bandgap highly crystalline polymer, PffBT4T-2DT can result in further improvements in device performance, with power conversion efficiencies approaching 10% and high open circuit voltages including very low voltage loss <0.5 V.[15] In this report, we focus on a comparison of blends of an analogous crystalline donor poly[(5,6-difluoro-2,1,3-benzothiadiazol-4,7-diyl)-alt-(3,3‴-di(2-octyldodecyl)-2,2′;5′,2″;5″,2‴-quaterthiophen-5,5‴-diyl)] (PffBT4T-2OD)[16] with [6,6]-phenyl C_{71} butyric acid methyl ester ($PC_{71}BM$) and with the nonfullerene small molecule EH-IDTBR (see the definition in Supporting information). Inverted PffBT4T-2OD:EH-IDTBR blend solar cell fabricated without any processing additive achieve PCEs of 9.5 ± 0.2%. The devices exhibit a high open circuit voltage of 1.08 ± 0.01 V, attributed to the high lowest unoccupied molecular orbital (LUMO) level of EH-IDTBR. Photoluminescence quenching and transient absorption data are employed to elucidate the ultrafast kinetics and efficiencies of charge separation in both blends, with PffBT4T-2OD exciton diffusion kinetics within polymer domains, and geminate recombination losses following exciton separation being identified as key factors determining the efficiency of photocurrent generation. Remarkably, while encapsulated PffBT4T-2OD:$PC_{71}BM$ solar cells show significant efficiency loss under simulated solar irradiation ("burn in" degradation) due to the trap-assisted recombination through increased photoinduced trap states, PffBT4T-2OD:EH-IDTBR solar cell shows negligible burn in efficiency loss. Furthermore, PffBT4T-2OD:EH-IDTBR solar cells are found to be substantially more stable under 85 °C thermal stress than PffBT4T-2OD:$PC_{71}BM$ devices.

The bulk heterojunction solar cells employed in this study use a nonfullerene small molecule EH-IDTBR[12–14] as the electron acceptor; for the donor, we employed a commercially available low bandgap polymer, PffBT4T-2OD,[16] which has high crystallinity and high molecular weight (M_n > 54 900, PDI = 2.14) (**Figure 1**a). We also prepared PffBT4T-2OD:$PC_{71}BM$-based solar cells as control samples. The devices were fabricated in an inverted configuration, using ZnO as an electron transport layer and MoO_3 as a hole transport layer (Figure 1b). For an optimized combination of PffBT4T-2OD and EH-IDTBR blend in the active layer, we adjusted the thermal annealing temperature and modified the film morphology with the various solvents (Table S1, Supporting Information). For devices based on EH-IDTBR, we obtained optimal device performance with donor:acceptor mass ratio of 1:1.4 in dichlorobenzene without any processing additives (tests with processing additives did not result in any significant improvement in device performance). In contrast, efficient device performance was only obtained for PffBT4T-2OD:$PC_{71}BM$ devices using a chlorobenzene:dichlorobenzene (1:1) mixed solvent in the presence of the processing additive DIO (a high boiling point solvent in which $PC_{71}BM$ is highly soluble), as reported previously.[16] The current density voltage (J–V) curves for optimized PffBT4T-2OD:EH-IDTBR and PffBT4T-2OD:$PC_{71}BM$ solar cells are shown in Figure 1c. The device parameters are listed in Table S1 in the Supporting Information, including consideration of performance reproducibility. Overall the PffBT4T-2OD:EH-IDTBR solar cell exhibits efficiencies up to 9.5 ± 0.2%, while the PffBT4T-2OD:$PC_{71}BM$ solar cells exhibited efficiencies up to 10.9 ± 0.1% with DIO. PffBT4T-2OD:$PC_{71}BM$ solar cells processed without DIO exhibited efficiencies of only up to 6.6% and poorer reproducibility, and will not be considered further herein. The devices employing EH-IDTBR exhibited higher voltages than device employing $PC_{71}BM$, attributed primarily to the higher LUMO energy of EH-IDTBR, as we have discussed in more detail for analogous devices elsewhere,[15] but lower photocurrents, as discussed below.

The UV–vis absorption spectra of the PffBT4T-2OD:EH-IDTBR and PffBT4T-2OD:$PC_{71}BM$ blends are shown in **Figure 2**a, respectively. Figure 1d displays the external quantum efficiency (EQE) spectra for both devices. PffBT4T-2OD:$PC_{71}BM$-based devices show broad and strong photoresponse from 350 to 800 nm, which is consistent with their broad UV–vis absorption spectrum. Compared with the PffBT4T-2OD:$PC_{71}BM$-based solar cells, the PffBT4T-2OD:EH-IDTBR solar cells show a significant decrease in the photoresponse at around 500 nm due to the lack of absorption of both photoactive materials. We also note that optimized EH-IDTBR devices have thinner film thicknesses than $PC_{71}BM$ (≈70 and ≈200 nm, respectively), which further contributes to the weak light absorption of the PffBT4T-2OD:EH-IDTBR solar cells around 500 nm. The integrated short circuit current (J_{SC}) values from these EQE data for PffBT4T-2OD:$PC_{71}BM$ and PffBT4T-2OD:EH-IDTBR are 18.7 and 14.0 mA cm^{-2}, respectively, in agreement (within 5% of the measured J_{SC} values. Overall, we can conclude that the more limited absorption range covered by the PffBT4T-2OD:EH-IDTBR blend, due to the overlap of the EH-IDTBR and PffBT4T-2OD absorption bands, is the primary cause of the lower J_{SC}. Despite this poorer light harvesting, it is striking that these devices still yield device efficiencies of 9.5%, suggesting that further tuning of energy levels to yield complimentary absorption bands is a promising route to further enhance device efficiencies.

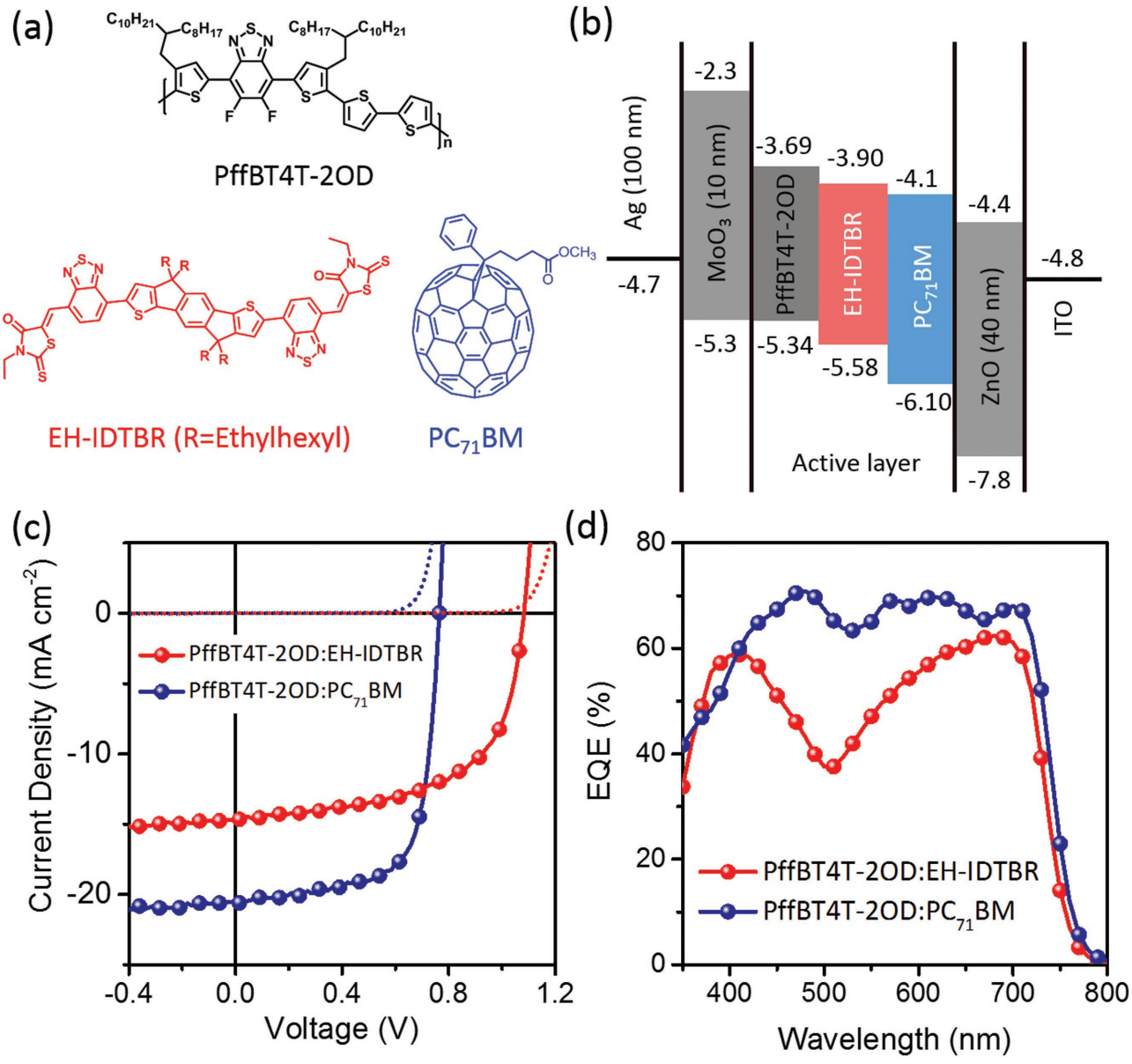

Figure 1. a) Chemical structures of PffBT4T-2OD as an electron acceptor and EH-IDTBR and $PC_{71}BM$ as electron acceptors, b) Energy levels of the materials used in this work from thin films;[13,14] HOMO levels measured by cyclic voltammetry and LUMO levels calculated based on HOMO levels and optical bandgaps, c) the *J–V* curve of PffBT4T-2OD-based solar cells, and d) the EQE curve of PffBT4T-2OD-based solar cells.

Photoluminescence (PL) studies were carried out on the PffBT4T-2OD:EH-IDTBR and PffBT4T-2OD:$PC_{71}BM$ blends as shown in Figure 2b. The polymer PL quenching efficiencies (PLQE) are similar for both blends: 80% for PffBT4T-2OD:EH-IDTBR and 77% for PffBT4T-2OD:$PC_{71}BM$. These relatively modest PL quenching efficiencies can be attributed most probably to the high crystallinity and large domain size of PffBT4T-2OD,[16] resulting in significant polymer exciton decay to ground during exciton diffusion to the polymer/acceptor interface. This exciton decay to ground corresponds to an ≈20% quantum efficiency loss, and is likely to be the primary cause of the subunity maximal EQE data shown in Figure 1d.

To investigate further charge generation and recombination dynamics in the two blend films studied herein, femtosecond transient absorption spectroscopy was employed (Figure 2c,d). We used an excitation wavelength of 715 nm for both thin films, corresponding to the PffBT4T-2OD absorption maximum, although we note that EH-IDTBR also absorbs at this wavelength. Transient absorption spectra as a function of time delay for both blend films are shown in Figure S2 in the Supporting Information, the corresponding control data for neat films are shown in Figure S1 in the Supporting Information. Figure 2c plots the transient absorption decay dynamics of neat PffBT4T-2OD, PffBT4T-2OD:EH-IDTBR, and PffBT4T-2OD:$PC_{71}BM$ films monitored at 1250 nm, assigned to the decay kinetics of PffBT4T-2OD singlet excitons (at this wavelength both EH-IDTBR excitons and the blend polarons yield relatively small signals, see the Supporting Information for

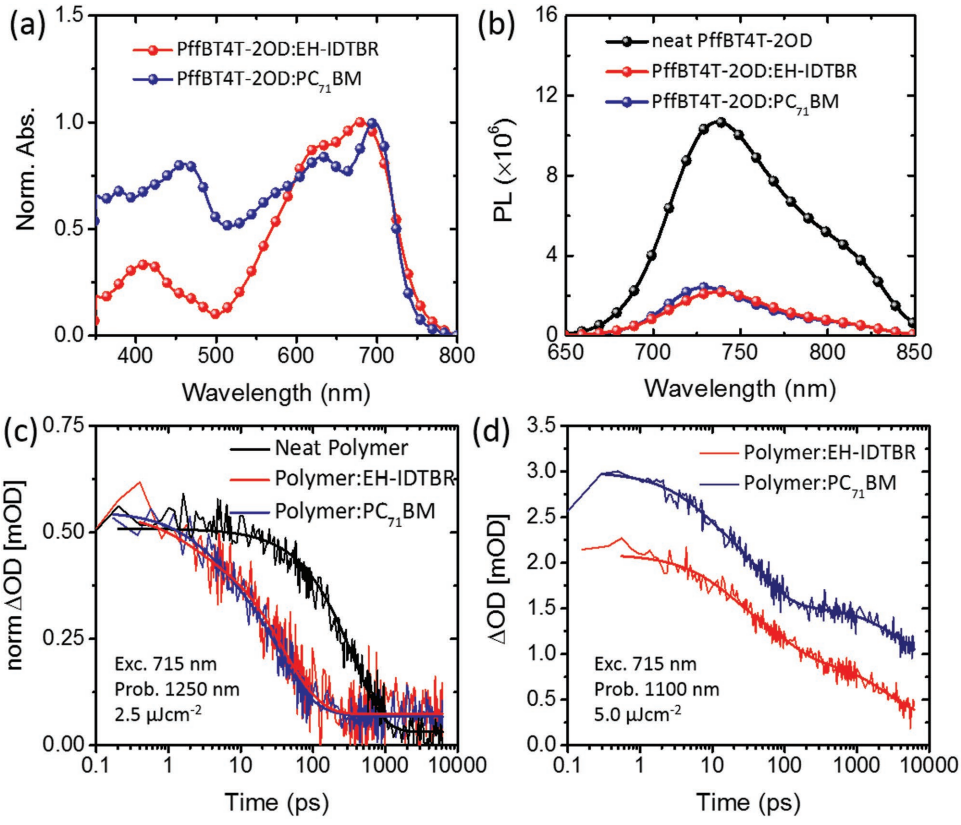

Figure 2. a) Normalized UV–vis absorption spectra and b) PL spectra excited at 715 nm for neat PffBT4T-2OD and PffBT4T-2OD:$PC_{71}BM$ and PffBT4T-2OD:EH-IDTBR blend films. c) Transient absorption data showing the time evolution of PffBT4T-2OD singlet exciton absorption probed at 1250 nm for the corresponding films (normalized at 1 ps) and d) showing the time evolution of singlet exciton (up to ≈100 ps) and polaron absorption (after ≈100 ps) for PffBT4T-2OD:$PC_{71}BM$ and PffBT4T-2OD:EH-IDTBR blends probed at 1100 nm (normalized for photons absorbed). The solid lines are the exponential decay fitting of absorption.

details). In the absence of acceptor, these excitons decay with a half-time of 280 ± 10 ps (2.5 μJ cm^{-2}), accelerating to half-times of 30 ± 0.5 and 28 ± 0.5 ps in blends with $PC_{71}BM$ and EH-IDTBR, respectively. These accelerated exciton decays, assigned to exciton quenching due to electron transfer to the molecular acceptors, are in reasonable agreement with the PL quenching efficiencies measured above (PLQE of 77% and 80% for blends with $PC_{71}BM$ and EH-IDTBR, respectively). This agreement, and the observation of a single exciton decay phase, indicate that PffBT4T-2OD in the blend films is primarily in pure polymer domains, with relatively little molecular scale mixing with the molecular acceptors. These data support our conclusion above that PffBT4T-2OD exciton decay to ground during diffusion within pure polymer domains results in a 10%–20% quantum efficiency loss in these devices.

While the PffBT4T-2OD exciton separation kinetics are very similar for both blend films, the yields and lifetimes of the photogenerated charges resulting from this exciton separation are clearly distinct. This can be observed from the amplitude of the PffBT4T-2OD polaron absorption observed centered at 1100 nm at long time delays in both films in Figure S2a,b in the Supporting Information, and illustrated must clearly as the slow decay phase in the transient kinetics plotted at this wavelength in Figure 2d (the initial decay phase is assigned to the decay of exciton absorption). It is apparent that compared to PffBT4T-2OD:$PC_{71}BM$ blends, PffBT4T-2OD:EH-IDTBR blend shows a lower amplitude and shorter life-time for this polaron signal (this plot is normalized for matched densities of absorbed photons). For both blends, these polaron decays apparent from 1 to 6 ns were found to be excitation intensity independent (Figure S2, Supporting Information) and therefore are assigned primarily to geminate recombination (at higher excitation densities, the decays become excitations density dependent, assigned to nongeminate recombination becoming faster than geminate recombination). It thus appears that geminate recombination losses are more significant for PffBT4T-2OD:EH-IDTBR than for PffBT4T-2OD:$PC_{71}BM$. The importance of geminate (monomolecular) recombination losses rather than nongeminate (bimolecular) recombination losses in limiting J_{SC} was supported by plots of J_{SC} versus light intensity (I), which indicate almost linear behavior for both devices ($J_{SC} \sim I^{\beta}$, $\beta \geq 0.98$ up to 1 sun). These increased geminate recombination losses most likely result from the high LUMO level of EH-IDTBR resulting in a lower energy offset driving charge separation (several studies have reported that lower energy offsets primarily cause increased geminate recombination losses rather than slower or less efficient exciton separation).[17] Increased geminate recombination losses for the EH-IDTBR blend are likely to be an additional factor limiting photocurrent generation and EQE values for these devices

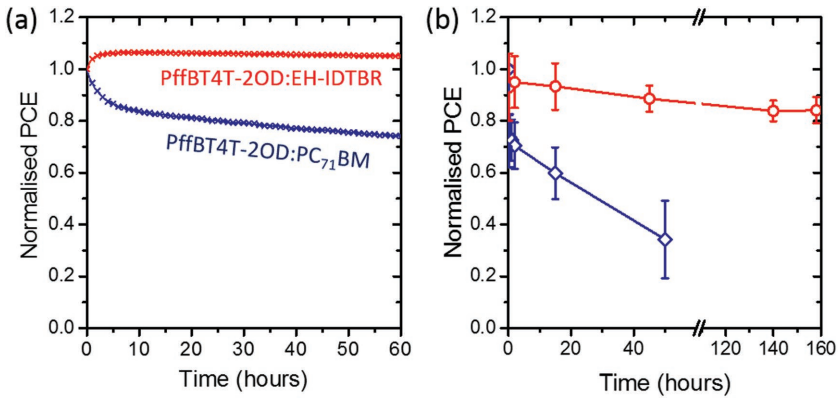

Figure 3. Normalized PCEs of the devices after long-term a) light soaking without UV light maintained below 50 °C thermal stress and b) annealing at 85 °C, under nitrogen.

fabricated with this blend, although a quantitative analysis of this issue would require consideration of the field dependence of these geminate recombination losses, beyond the scope of this study.

We turn now to consideration of the stability of PffBT4T-2OD:PC_{71}BM and PffBT4T-2OD:EH-IDTBR solar cells. Device stability was tested for glass encapsulated devices under light or thermal stress and unencapsulated devices under dark in air. Normalized power conversion efficiency (PCE) data are shown in **Figure 3**, with full device characteristics detailed in Figures S3 and S4 in the Supporting Information. Under white light stress, the PCE of a representative PffBT4T-2OD:PC_{71}BM-based device, decreased up over 20% over 60 h, typical of light induced burn in losses reported for other OSC employing fullerene acceptors.[3] In contrast, the PffBT4T-2OD:EH-IDTBR device shows essentially no light induced efficiency loss over this timescale, exhibiting a PCE of 9.5 ± 0.2% after 60 h under illumination indeed in some cases a modest increase in performance was observed, attributed to photoinduced doping of the ZnO layer.[18] This difference in burn-in response was tested for 18 devices, in all tests the PffBT4T-2OD:EH-IDTBR showed substantially less or negligible burn in efficiency loss compared to PffBT4T-2OD:PC_{71}BM devices (normalized PCE losses after 60 h of 0 ± 4% and –26 ± 8%, respectively). Under 85 °C thermal stress in the dark, the PffBT4T-2OD:EH-IDTBR device also showed substantially improved stability compared to PffBT4T-2OD:PC_{71}BM devices (Figure 3b), with the EH-IDTBR showing a normalized PCE loss of only 16 ± 4% after 160 h of thermal loss, while that of the PffBT4T-2OD:PC_{71}BM-based device dropped 73 ± 15% within 60 h. We note that the loss of device performance with PC_{71}BM showed clearly different origins under light and thermal stress. Under light stress, PCE loss derived primarily from loss of fill factor (FF), indicative of increased charge trapping and recombination.[6] Under thermal stress, PCE loss derived primarily from a loss of J_{SC}, indicative of thermally induced phase segregation.[6,8] Supporting this conclusion for the origin of thermally induced efficiency loss, atomic force microscopy (AFM) data indicate a significant increase in film roughness following thermal stress for PffBT4T-2OD:PC_{71}BM but not for PffBT4T-2OD:EH-IDTBR (see Figure S5 in the Supporting Information), and optical microscopy images indicate the formation of micrometre-sized clusters after thermal stress at 85 °C for 12 h for PffBT4T-2OD:PC_{71}BM blend films, which were not observed for PffBT4T-2OD:EH-IDTBR blend films (see Figure S6 in the Supporting Information). Consistent with this conclusion, we note that Brabec and coworkers have recently reported that PffBT4T-2OD:PC_{61}BM blends can be susceptible to J_{SC} loss due to spinodal demixing, consistent with the thermal degradation we observe herein but distinct from the FF loss we observe under light induced degradation.[7] We also tested the ambient shelf life stability of unencapsulated PffBT4T-2OD:EH-IDTBR and PffBT4T-2OD:PC_{71}BM devices. Devices were stored at room temperature under dark conditions. After 95 h of air exposure, PffBT4T-2OD:EH-IDTBR devices lost ≈28% of their initial PCE, whereas PffBT4T-2OD:PC_{71}BM devices performance lost 85% of their initial PCE after 65 h (Figure S7, Supporting Information). These results suggest that PffBT4T-2OD:EH-IDTBR devices exhibit not only improved resistance to thermal and light stress but also superior shelf-life performance under ambient exposure.

Figure 3 indicates that PffBT4T-2OD:EH-IDTBR devices are significantly more stable under both light and thermal stress conditions than PffBT4T-2OD:PC_{71}BM devices, and in particularly show negligible burn in efficiency loss. The remarkable stability of PffBT4T-2OD:EH-IDTBR devices was found to be rather specific to this combination of donor and acceptor materials, with for example, PffBT4T-2OD devices fabricated with some alternative rhodanine acceptors to EH-IDTBR showing greater burn-in efficiency losses, as we will report in detail elsewhere. We note that unlike the PffBT4T-2OD:PC_{71}BM devices studied herein, the EH-IDTBR devices were fabricated without the DIO processing additive, which may in part explain the improved thermal stability. We also note that EH-IDTBR, in contrast to PC_{71}BM, shows significant crystallinity,[13] which is also likely to be a factor in the improved thermal stability of EH-IDTBR devices.[1a]

To investigate further the origin of the burn-in degradation observed herein, charge extraction (CE) and transient photovoltage (TPV) measurements were undertaken to determine the charge carrier densities and recombination dynamics of fresh and aged solar cells. For PffBT4T-2OD:PC_{71}BM, these CE data, **Figure 4**a, indicate an ≈50% increase in charge carrier density for matched cell open circuit voltage (V_{OC})'s and therefore matched quasi-Fermi level splitting. As this charge carrier density is primarily in shallow trap states, this increase in charge density indicates that light induced burn in efficiency loss correlates with a 50% increase in the density of electronic trap states. This conclusion is supported by our observation of increased carrier lifetimes following burn in Figure 4b, indicative of increased charge trapping, and is also consistent with our observation that burn in efficiency loss primarily results from a loss of FF, indicative of a loss of collection efficiency. In contrast, for PffBT4T-2OD:EH-IDTBR devices (Figure S9, Supporting Information), both CE and TPV measurements were observed to be relatively insensitive to device light exposure.

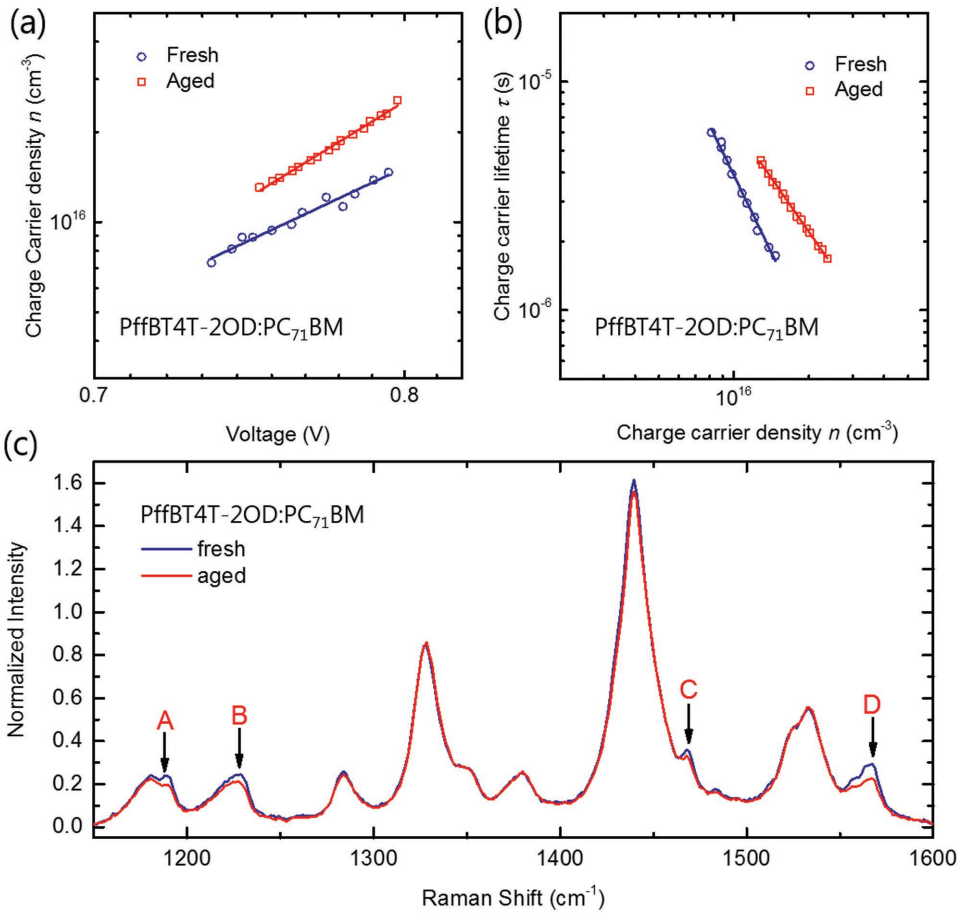

Figure 4. Transient optoelectronic analyses of PffBT4T-2OD:$PC_{71}BM$ device before and after light induced burn in efficiency loss. a) Charge extraction (CE) measurements of charge carrier density at open circuit as a function of light intensity, plotted versus open circuit voltage; b) the corresponding charge carrier lifetimes measured by transient photovoltage (TPV) decays, plotted against the measured charge densities. Device aging (burn in) was induced by the 540 nm light source employed in the CE and TPV measurements. c) Representative Raman spectra of fresh and light-aged PffBT4T-2OD:$PC_{71}BM$ blend layer of devices, obtained via 488 nm laser excitation and normalized to polymer-only peak at 850 cm^{-1}. Peaks labeled A–D are signatures of $PC_{71}BM$. Light aging employed 4 h LED white light irradiation as for Figure 3a.

These results were supported by ideality factor measurements, which indicate a modest increase in ideality factor for light aged PffBT4T-2OD:$PC_{71}BM$ devices, as expected for increased charge trapping following light exposure (Figure S8, Supporting Information).[2d,6b]

We turn now to the molecular origin of improved resistance of PffBT4T-2OD:EH-IDTBR devices to light induced charge trapping, and associated burn in performance loss. We note that, unlike $PC_{61}BM$, $PC_{71}BM$ is resistant to photoinduced dimerization, so that differences in photoinduced dimerization are unlikely to explain the improved stability. AFM data indicates that the increase in trap density for light exposed PffBT4T-2OD:$PC_{71}BM$ is not associated with a change in film morphology (Figure S10, Supporting Information). In contrast, Raman spectra (Figure 4c) indicate that light exposure results in specific loss of four $PC_{71}BM$ Raman features which are light induced degradation sites, while those of PffBT4T-2OD are unchanged (see Raman spectra of neat PffBT4T-2OD and $PC_{71}BM$ films in Figure S11 in the Supporting Information, respectively). In particular, 4 h LED light exposure results in 23% loss of a Raman feature at 1565 cm^{-1} (marked as Feature D in Figure 4c) assigned previously to localized vibrations of C_5/C_6 rings of the fullerene cage.[19] We note that no frequency shifts in Raman features were observed, confirming negligible fullerene cage dimerization; similarly these Raman spectra rule out significant photooxidation of the C_{70} cage.[20] Specific reduction of the 1565 cm^{-1} Raman feature, with the other features being relatively invariant, is most likely not due to fullerene segregation but rather light induced bond disruption or cleavage at the site of the solubilizing side group attachment to the C_{70} cage. While further work is clearly required to understand fully these observations, these data suggest that light induced burn in efficiency loss in the PffBT4T-2OD:$PC_{71}BM$ devices studied herein is associated with photoinduced degradation of $PC_{71}BM$, with EH-IDTBR being less susceptible to such degradation.

In summary, we conclude that the improved stability of PffBT4T-2OD:EH-IDTBR devices to light induced burn in efficiency loss is correlated with a greater resistance to photoinduced electronic trap state formation relative to devices employing $PC_{71}BM$. We note that McGehee and co-workers have also observed that burn in efficiency losses are correlated with trap state formation and that these losses were reduced for

more crystalline materials.[6] Clearly the stability data we report herein is limited in scope and timescale, and further work is required to elucidate fully the relationships between trap state formation, material structure and crystallinity, the use of processing additives, and stability for the materials studied herein. However, the data herein demonstrate that, at least under the conditions studied, PffBT4T-2OD:EH-IDTBR devices show remarkably stability, significantly superior to that of PffBT4T-2OD:$PC_{71}BM$ devices, which is promising for future applications of this new NFA.

Supporting Information

Supporting Information is available from the Wiley Online Library or from the author.

Acknowledgements

The authors gratefully acknowledge funding supported by KAUST under the Grant Agreement number OSR-2015-CRG4-2572, the EU FP7 project CHEETAH, the EPSRC through the Centre for Doctoral Training in Plastic Electronics (EP/L0160702/1) and thank Pabitra Shakya for assistance in device fabrication.

Conflict of Interest

The authors declare no conflict of interest.

Keywords

charge separation, nonfullerene acceptors, organic solar cells, trap assisted recombination

Received: February 27, 2017
Revised: April 28, 2017
Published online: June 28, 2017

[1] a) P. Cheng, X. Zhan, *Chem. Soc. Rev.* **2016**, *45*, 2544; b) I. F. Domínguez, A. Distler, L. Lüer, *Adv. Energy Mater.* **2016**, *7*, 1601320. c) S. Savagatrup, A. D. Printz, T. F. O'Connor, A. V. Zaretski, D. Rodriquez, E. J. Sawyer, K. M. Rajan, R. I. Acosta, S. E. Root, D. J. Lipomi, *Energy Environ. Sci.* **2015**, *8*, 55.

[2] a) C. H. Peters, I. T. Sachs-Quintana, W. R. Mateker, T. Heumueller, J. Rivnay, R. Noriega, Z. M. Beiley, E. T. Hoke, A. Salleo, M. D. McGehee, *Adv. Mater.* **2012**, *24*, 663; b) X. Wen, Y. Feng, S. Huang, F. Huang, Y.-B. Cheng, M. Green, A. Ho-Baillie, *J. Mater. Chem. C* **2016**, *4*, 793; c) A. Aguirre, S. C. J. Meskers, R. A. J. Janssen, H. J. Egelhaaf, *Org. Electron.* **2011**, *12*, 1657; d) T. Heumueller, W. R. Mateker, I. T. Sachs-Quintana, K. Vandewal, J. A. Bartelt, T. M. Burke, T. Ameri, C. J. Brabec, M. D. McGehee, *Energy Environ. Sci.* **2014**, *7*, 2974.

[3] a) R. Roesch, K. R. Eberhardt, S. Engmann, G. Gobsch, H. Hoppe, *Sol. Energy Mater. Sol. Cells* **2013**, *117*, 59; b) T. M. Clarke, C. Lungenschmied, J. Peet, N. Drolet, K. Sunahara, A. Furube, A. J. Mozer, *Adv. Energy Mater.* **2013**, *3*, 1473; c) S. A. Gevorgyan, M. V. Madsen, B. Roth, M. Corazza, M. Hösel, R. R. Søndergaard, M. Jørgensen, F. C. Krebs, *Adv. Energy Mater.* **2016**, *6*, 1501208.

[4] a) S. Gamerith, C. Gadermaier, H. G. Nothofer, U. Scherf, E. J. List, *Proc. SPIE* **2004**, *5464*, 104; b) S. Cros, M. Firon, S. Lenfant, P. Trouslard, L. Beck, *Nucl. Instrum. Methods Phys. Res., Sect. B* **2006**, *251*, 257.

[5] a) M. M. Roubelakis, G. C. Vougioukalakis, L. C. Nye, T. Drewello, M. Orfanopoulos, *Tetrahedron* **2010**, *66*, 9363; b) K. P. Meletov, J. Arvanitidis, D. Christofilos, G. A. Kourouklis, V. A. Davydov, *Chem. Phys. Lett.* **2016**, *654*, 81.

[6] a) T. Heumueller, W. R. Mateker, A. Distler, U. F. Fritze, R. Cheacharoen, W. H. Nguyen, M. Biele, M. Salvador, M. von Delius, H.-J. Egelhaaf, M. D. McGehee, C. J. Brabec, *Energy Environ. Sci.* **2016**, *9*, 247; b) T. Heumueller, T. M. Burke, W. R. Mateker, I. T. Sachs-Quintana, K. Vandewal, C. J. Brabec, M. D. McGehee, *Adv. Energy Mater.* **2015**, *5*, 1500111; c) Z. M. Beiley, E. T. Hoke, R. Noriega, J. Dacuña, G. F. Burkhard, J. A. Bartelt, A. Salleo, M. F. Toney, M. D. McGehee, *Adv. Energy Mater.* **2011**, *1*, 954.

[7] N. Li, J. D. Perea, T. Kassar, M. Richter, T. Heumueller, G. J. Matt, Y. Hou, N. S. Güldldal, H. Chen, S. Chen, S. Langner, M. Berlinghof, T. Unruh, C. J. Brabec, *Nat. Commun.* **2016**, *8*, 14541.

[8] a) B. C. Schroeder, Z. Li, M. A. Brady, G. C. Faria, R. S. Ashraf, C. J. Takacs, J. S. Cowart, D. T. Duong, K. H. Chiu, C.-H. Tan, J. T. Cabral, A. Salleo, M. L. Chabinyc, J. R. Durrant, I. McCulloch, *Angew. Chem., Int. Ed.* **2014**, *53*, 12870; b) Z. Li, K. H. Chiu, R. S. Ashraf, S. Fearn, R. Dattani, H. C. Wong, C. H. Tan, J. Wu, J. T. Cabral, J. R. Durrant, *Sci. Rep.* **2014**, *5*, 15149; c) H. C. Wong, Z. Li, C. H. Tan, H. Zhong, Z. Huang, H. Bronstein, I. McCulloch, J. T. Cabral, J. R. Durrant, *ACS Nano* **2014**, *8*, 1297.

[9] B. J. Tremolet de Villers, K. A. O'Hara, D. P. Ostrowski, P. H. Biddle, S. E. Shaheen, M. L. Chabinyc, D. C. Olson, N. Kopidakis, *Chem. Mater.* **2016**, *28*, 876.

[10] a) W. Zhao, D. Qian, S. Zhang, S. Li, O. Inganäs, F. Gao, J. Hou, *Adv. Mater.* **2016**, *28*, 4734; b) Y. Lin, J. Wang, Z. G. Zhang, H. Bai, Y. Li, D. Zhu, X. Zhan, *Adv. Mater.* **2015**, *27*, 1170; c) Lin, F. Zhao, Q. He, L. Huo, Y. Wu, T. C. Parker, W. Ma, Y. Sun, C. Wang, D. Zhu, A. J. Heeger, *J. Am. Chem. Soc.* **2016**, *138*, 4955; d) Y. Lin, Q. He, F. Zhao, L. Huo, J. Mai, X. Lu, C. J. Su, T. Li, J. Wang, J. Zhu, Y. Sun, *J. Am. Chem. Soc.* **2016**, *138*, 2973.

[11] a) S. Shoaee, F. Deledalle, P. Shakya Tuladhar, R. Shivanna, S. Rajaram, K. S. Narayan, J. R. Durrant, *J. Phys. Chem. Lett.* **2015**, *6*, 201; b) Y. J. Hwang, B. A. Courtright, A. S. Ferreira, S. H. Tolbert, S. A. Jenekhe, *Adv. Mater.* **2015**, *27*, 4578; c) H. Li, Y. J. Hwang, B. A. Courtright, F. N. Eberle, S. Subramaniyan, S. A. Jenekhe, *Adv. Mater.* **2015**, *27*, 3266.

[12] S. Holliday, R. S. Ashraf, C. B. Nielsen, M. Kirkus, J. A. Röhr, C. H. Tan, E. Collado-Fregoso, A. C. Knall, J. R. Durrant, J. Nelson, I. McCulloch, *J. Am. Chem. Soc.* **2015**, *137*, 898.

[13] S. Holliday, R. S. Ashraf, A. Wadsworth, D. Baran, S. A. Yousaf, C. B. Nielsen, C. H. Tan, S. D. Dimitrov, Z. Shang, N. Gasparini, M. Alamoudi, F. Laquai, C. J. Brabec, A. Salleo, J. R. Durrant, I. McCulloch, *Nat. Commun.* **2016**, *7*, 11585.

[14] D. Baran, R. S. Ashraf, D. A. Hanifi, M. Abdelsamie, N. Gasparini, J. A. Röhr, S. Holliday, A. Wadsworth, S. Lockett, M. Neophytou, C. J. Emmott, J. Nelson, C. J. Brabec, A. Amassian, A. Salleo, T. Kirchartz, J. R. Durrant, I. McCulloch, *Nat. Mater.* **2016**, *16*, 363.

[15] D. Baran, T. Kirchartz, S. Wheeler, S. Dimitrov, M. Abdelsamie, J. Gorman, R. S. Ashraf, S. Holliday, A. Wadsworth, N. Gasparini, P. Kaienburg, H. Yan, A. Amassian, C. J. Brabec, J. R. Durrant, I. McCulloch, *Energy Environ. Sci.* **2016**, *9*, 3783.

[16] Y. Liu, J. Zhao, Z. Li, C. Mu, W. Ma, H. Hu, K. Jiang, H. Lin, H. Ade, H. Yan, *Nat. Commun.* **2014**, *5*, 5293.

[17] a) J. Liu, S. Chen, D. Qian, B. Gautam, G. Yang, J. Zhao, J. Bergqvist, F. Zhang, W. Ma, H. Ade, O. Inganäs, K. Gundogdu, F. Gao, H. Yan, *Nat. Energy* **2016**, *1*, 16089; b) S. D. Dimitrov, J. R. Durrant, *Chem. Mater.* **2014**, *26*, 616.

[18] a) S. A. Gevorgyan, N. Espinosa, L. Ciammaruchi, B. Roth, F. Livi, S. Tsopanidis, S. Züfle, S. Queirós, A. Gregori, G. A. DosReis Benatto, M. Corazza, M. V. Madsen, M. Hösel, M. J. Beliatis, T. T. Larsen-Olsen, F. Pastorelli, A. Castro, A. Mingorance, V. Lenzi, D. Fluhr, R. Roesch, M. M. D. Ramos, A. Savva, H. Hoppe, L. S. A. Marques, I. Burgués, E. Georgiou, L. Serrano-Luján, F. C. Krebs, *Adv. Energy Mater.* **2016**, *6*, 1600910; b) B. A. MacLeod, B. J. Tremolet de Villers, P. Schulz, P. F. Ndione, H. Kim, A. J. Giordano, K. Zhu, S. R. Marder, S. Graham, J. J. Berry, A. Kahn, D. C. Olson, *Energy Environ. Sci.* **2015**, *8*, 592; c) W.-Y. Jin, R. T. Ginting, S.-H. Jin, J.-W. Kang, *J. Mater. Chem. A* **2016**, *4*, 3784; d) A. Chapel, S. B. Dkhil, S. Therias, J.-L. Gardette, D. Hannani, G. Poize, M. Gaceur, S. M. Shah, P. Wong-Wah-Chung, C. Videlot-Ackermann, O. Margeat, A. Rivaton, J. Ackermann, *Sol. Energy Mater. Sol. Cells* **2016**, *155*, 79.
[19] V. Schettino, M. Pagliai, G. Cardini, *J. Phys. Chem. A* **2002**, *106*, 1815.
[20] Y. Wang, J. M. Holden, Z.-H. Dong, X.-X. Bi, P. C. Eklund, *Chem. Phys. Lett.* **1993**, *211*, 341.

